Processing Multi-Spectral Scanning Electron Microscopy Images for Quantitative Microfabric Analysis

N. K. Tovey
University of East Anglia, e680@uk.ac.uea.cpcvax

D. L. Dent
University of East Anglia

W. M. Corbett
University of East Anglia

D. H. Krinsley
University of Oregon

Recommended Citation

Utah State University
MERRILL-CAZIER LIBRARY

PROCESSING MULTI-SPECTRAL SCANNING ELECTRON MICROSCOPY IMAGES FOR QUANTITATIVE MICROFABRIC ANALYSIS

N.K. Tovey[1*], D.L. Dent[1], W.M. Corbett[1], and D.H. Krinsley[2]

[1]School of Environmental Sciences, University of East Anglia, Norwich, NR4 7TJ, U.K.
[2]Department of Geological Sciences, University of Oregon, Eugene, Oregon, 97403-1272, USA.

Abstract

Multi-spectral image analysis is a powerful method to characterise quantitatively the mineralogy and microfabric of soils, sediments, and other particulate materials. Back-scattered scanning electron microscope (SEM) images of polished, resin-impregnated samples are grouped with the corresponding X-ray elemental maps using classification methods commonly used in remote sensing. However, the resulting *mineral-segmented* images require processing to render them suitable for quantification. In the past, this has been done subjectively and interactively, but the new objective methods described in this paper largely eliminate this subjectivity. An intensity gradient magnitude image of the original back-scattered electron image is used as the basis of an interactive erosion and dilation sequence to generate skeleton outlines defining the edges of the mineral grains. The areas defined within the skeleton areas are then classified as a particular mineral according to the predominant feature in the corresponding mineral-segmented image. Subsequent processing tackles the problems of 'holes' defined by the skeleton outlines, and the over-segmentation associated with certain classes of mineral grain. Further methods to deal with particles made up of more than one mineral are considered.

The matrix and porosity information is recombined to generate an image suitable for analysis using feature size statistics or general orientation analysis. The techniques described can be combined to permit batch processing of images. Applications of the techniques are illustrated on a soil from the East Anglian Breckland.

* Address for correspondence:
N. K. Tovey
School of Environmental Sciences,
University of East Anglia,
Norwich, NR4 7TJ
U.K.

Telephone: 44 (0)603 56161
FAX No: 44 (0)603 501179
E-Mail: e680@uk.ac.uea.cpcvax

Introduction

Over the last 20 years, multi-spectral classification methods have been developed to interpret satellite images. Usually, these methods rely on the specification, by the operator, of a training region representative of the feature of interest. In the last few years, similar methods have been applied to microscopic images (e.g. Protz et al, 1992).

Most soils and sediments consist of particles having different mineralogies and covering a large range in the size of particles. Their microfabric, described by the spatial arrangement of the constituent particles and associated voids, plays an important role in determining the behaviour of the material as a whole. Knowledge of this microfabric is thus important for many purposes, for example: 1) to understand the diagenesis of the sediments, 2) to predict the response of the material to deformation, 3) to predict hydraulic behaviour, and 4) to predict crop yields. Considerable work has been done to study the microfabric of soils but, with some notable exceptions (e.g. Lafeber, 1967; Morgenstern and Tchalenko, 1967a,b; Foster and Evans, 1971; Tchalenko et al. 1971; Tovey, 1973a,b; Tovey and Wong, 1978), most observations have been qualitative. A comprehensive list of early work on quantification may be found in Smart and Tovey (1982).

In recent years, many methods of using image analysis have been developed, and there are several promising applications to soil micromorphology. A prime requirement in many methods is to determine a correct threshold to segment the image, in order to separate features of interest from those that are not. If this segmentation can be achieved reliably, then traditional feature analysis may be used to assess the size, shape and orientation of the larger mineral grains. Equally, assessments of the nature of porosity may be made using the mathematical morphological methods described by Erhlich et al. (1984). Finally, methods which assess intensity differences and, thus, do not require prior segmentation, may be used to study the orientation of the fine-grained material (Smart and Tovey, 1988; Tovey et al. 1989, 1992a, 1992b).

For a complete quantitative analysis of microfabric, several techniques are needed. Some are more suited to the study of the larger grains and macro pores, others are more suited to study of the fine particles and pores. Therefore, it is necessary to segment images into those regions best suited to treatment by the different techniques.

Given a back-scattered scanning electron microscope (BSE)image of a polished, impregnated sample that is relatively free of noise and that has adequate contrast, it is often possible to select a threshold which will segment the image to separate correctly the large voids from the solid phase. The voids, filled with resin, have a lower mean atomic number
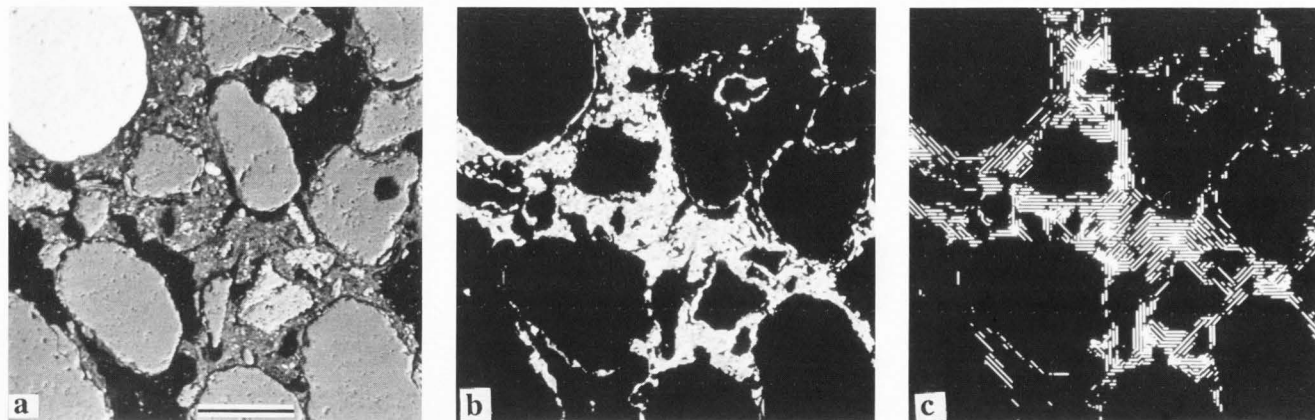
Fig. 1. Breckland Soil: a) BSE image; b) image after classification and removal of mineral grains to show clay matrix; c) orientation of domains in clay matrix. Fig. 1c represents the final point in the procedures described in this paper. Bar = 0.1 mm.
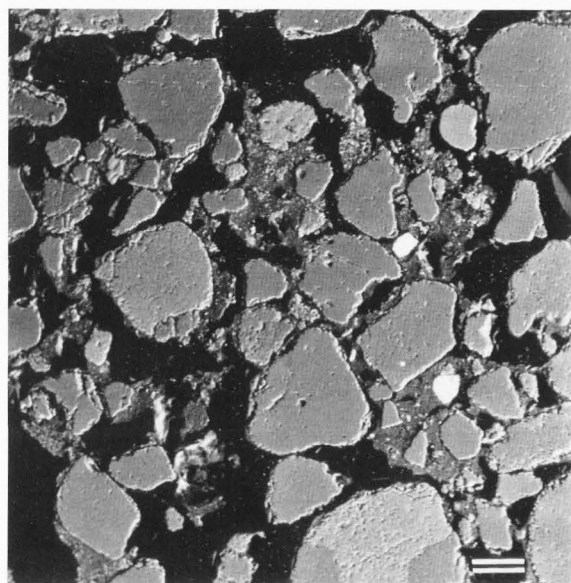

Fig. 2. Back-scattered electron image of the Breckland Soil used as an example to illustrate the procedures described in the paper. Bar = 0.1 mm.

Fig. 3. Map showing location of quartz and feldspar grains. Such a map is only obtained after the full processing. Bar = 0.1 mm.

and thus appear much darker. To enhance the objectivity of the selection of a threshold, particularly if batches of images are to examined routinely, a technique such as the weighted relative contrast histogram method described by Köhler (1981), may be used (Hounslow and Tovey, 1992).

Analysis of the shape, size, and orientation of the larger mineral grains is more difficult. In theory, it might be possible to use a multiple thresholding method (using the relative contrast histogram method) to detect differences in mean atomic number between one mineral and another. Thereby, the different mineral types might be segregated from each other and from the fine grained matrix. In practice, this cannot be achieved with real soils, such as shown in the image in Fig. 1, for reasons discussed later. Multi-spectral methods show promise in separating the different classes of mineral grains from each other and from the fine clay matrix. For this reason, the associated
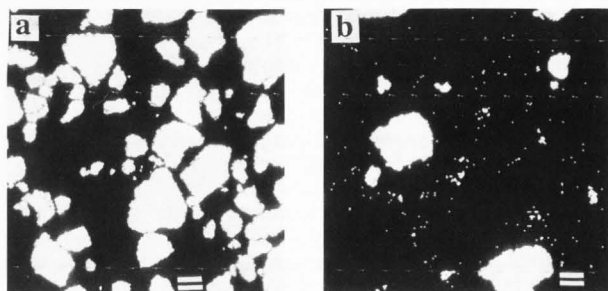
processing techniques described in this paper have been developed.

To illustrate the techniques, a sample from the interface between a layer of Pleistocene aeolian sand and underlying cryoturbated, chalky-sand drift was used. Subsequent leaching has dissolved most of the chalk flour mixed into the sand and washed iron-rich clay from the aeolian deposit into a distinct band at the interface between the two drifts. The clay appears to be associated with the residual chalk material within the pores.

The back-scattered electron image (Fig. 1a) shows a soil composed largely of silt and fine sand particles but, also, with clay and very fine silt within the interstitial pores, frequently as oriented cutans around the larger grains. If the clay matrix is the subject of study, then multi-spectral methods may be used to identify the larger mineral grains. Both these grains and the large voids can then be 'removed' from the image before quantitatively analysing the matrix. An outline of the areas covered by this matrix is shown in Fig. 1b. The orientation of features within this may be assessed using intensity gradient methods (e.g. Tovey et al, 1989). It is also possible to examine the extent of aggregation of particles into domains, and whether such domains have an orientation related to that of the larger mineral grains. Fig. 1c shows that the matrix is highly aligned following the grain surfaces, suggesting that there has been a flow of the clay matrix around the mineral grains. To conduct such analyses, it is necessary to classify the original image, using multi-spectral methods, and then process the resulting image until it is

suitable for further analysis. While this processing may be done interactively and subjectively, an objective method is needed if batch processing of images is to become feasible. It is this aspect that is addressed in this paper.

To illustrate the methods developed, and to highlight the technical difficulties that may be encountered, a second image that proved particularly difficult to process has been chosen (Fig. 2). The mineral grains are mostly either quartz or potassium feldspar but it is very difficult to differentiate between the two species in the back-scattered electron image. For clarity, the quartz grains and feldspar grains are identified in Fig. 3 although, in practice, it is only at the end of the full procedure that such segmented images can be produced.

Using Figs. 3a and 3b to mask separately the different mineral species, it is possible examine the range of grey-level intensities in each mineral. These are displayed in Fig. 4. The histogram for quartz is narrow and well defined, but that for feldspar is bi-modal and, furthermore, the lower peak coincides almost exactly with that of quartz. This makes it difficult to separate the two minerals from the back-scattered image alone. The back-scattered image, which should show predominantly chemical contrast, also shows some topographic contrast from pits in the feldspar grains, and this contributes to the spread of the grey level intensities in this mineral. The situation is further complicated by the fact that the range of intensities in the matrix also overlaps these other two ranges. Clearly, multiple thresholding methods cannot be used on materials such as this.

Multi-spectral methods were developed to study remotely-sensed satellite data from several different wavebands of visible and infra red radiation. If, in one waveband or a group of wavebands, a combination of intensities differentiates one feature from another, then this may be used in one of the standard classification routines. Digital back-scattered electron (BSE) images and X-ray maps showing the distribution of several key elements were obtained from each area of interest. Thus, several different image spectra from the same area were obtained and the standard multi-spectral classification methods could be used. Four separate mineral types were identified in this series, although as many as eight have been observed in other studies. While it is helpful to have a prior knowledge of the minerals present, this is not essential as selected characteristics may be identified by visually comparing the X-ray maps with each other and with the BSE image. In this particular image, several characteristics were noted:

a) regions with high intensities of silicon, but low intensities of other elements (identified as quartz);

b) regions with moderate to high concentrations of silicon associated with moderate concentrations of both potassium and aluminium (identified as potassium feldspar);

c) regions of high iron content in the absence of sulphur (identified as iron oxide);

d) high concentrations of calcium with no association with other elements (identified as chalk grains);

e) concentrations of calcium weaker than (iv), and also dispersed (interpreted as weathered chalk particles of matrix grain size diluted by presence of matrix);

f) weak to moderate concentrations of both aluminium and silicon dispersed as fine particles with no other elements (identified as the matrix of predominantly clay minerals).

Classification starts by highlighting a typical area in one of the minerals and using this as a training area to locate all grains of that mineral within the image. This classification generates a *mineral-segmented* image that shows the distribution of all identified mineral types. However, there are several residual problems with these segmented images
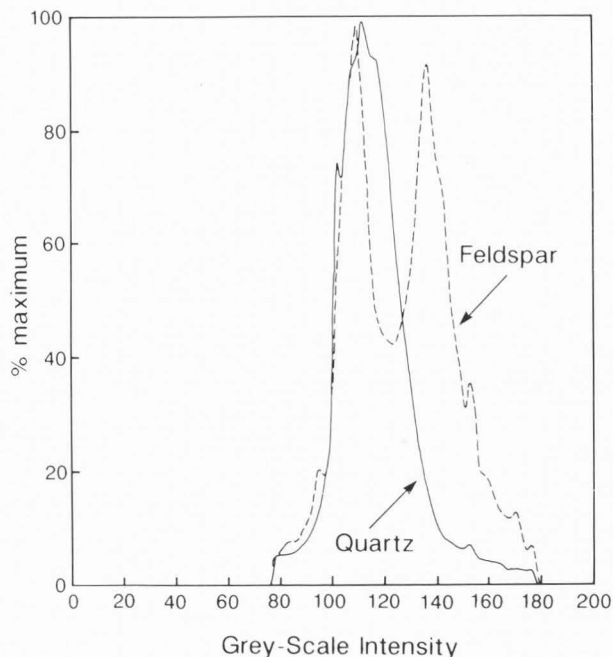

Fig. 4. Histograms showing grey-level distribution within the feldspar and quartz areas of Fig. 2. This was obtained using masks derived from Fig. 3.

that must be addressed to render them suitable for the subsequent analysis of particle size and shape and, also, to study quantitatively the fine-grained material. In previous work (Tovey and Krinsley, 1991,1992; Tovey et al 1992c), the mineral-segmented images were processed individually in an interactive manner by the operator until they 'looked right'. This procedure is subjective and does not permit the batch-processing of images. This paper describes an objective method for post-processing the mineral-segmented images. Particle size analyses can then be done on the separate mineral species, and the orientation of the larger grains may be examined with respect to the orientation within the matrix. Such factors can now be examined in a quantitative way not possible by other methods. While the techniques described in this paper relate to two-dimensional studies, there is no reason why some aspects of the technique could not be extended to three dimensions by observing orthogonal planes in each sample.

General Procedure

The general procedure is summarised in Fig. 5. It involves several stages, each of which involves several steps. The stages are:- 1) digital image acquisition and checking for image register; 2) selection of training areas typical of each mineral and the basic classification; 3) computation of a binary image of pores and modification of the raw classified image; 4) generation of an image representing the magnitude of the intensity gradient vector at each pixel, and the subsequent conversion of this image into a binary skeletal form; 5) the analysis of the skeleton image to define particle and void areas; 6) the segregation of the mineral grains from the matrix from the raw classified image and the establishment of a transformation matrix indicating the dominant mineral class present in each skeletal region; 7) the treatment of grains with more than one dominant mineral species; 8) the combination of adjoining grains to remove over-

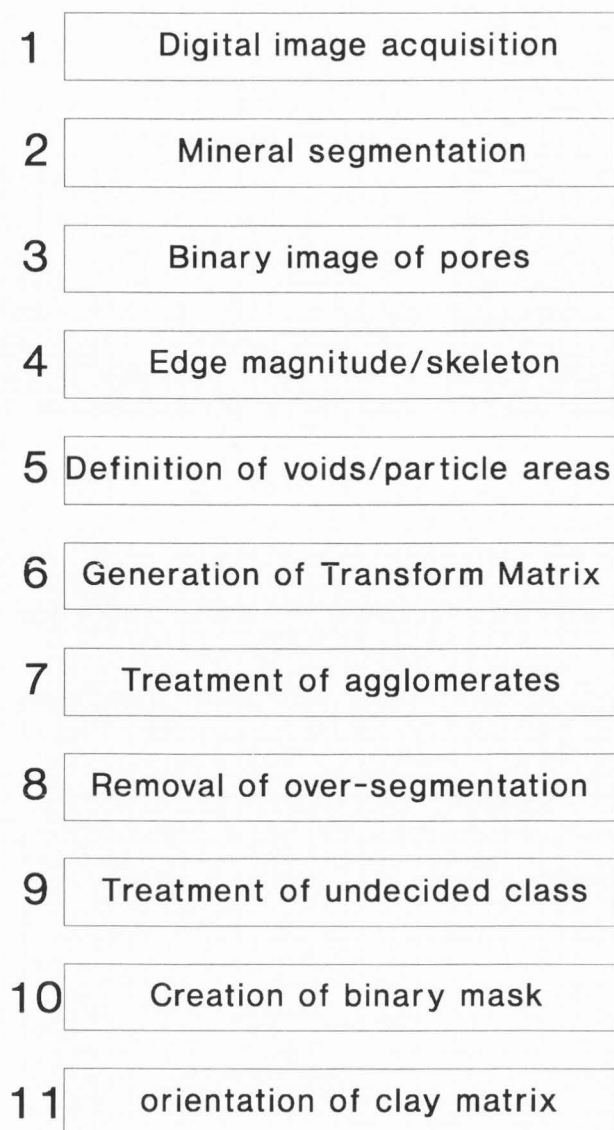|	
1	Digital image acquisition
2	Mineral segmentation
3	Binary image of pores
4	Edge magnitude/skeleton
5	Definition of voids/particle areas
6	Generation of Transform Matrix
7	Treatment of agglomerates
8	Removal of over-segmentation
9	Treatment of undecided class
10	Creation of binary mask
11	orientation of clay matrix

Fig. 5. Flow chart showing the steps in the process.

segmentation, and the removal of holes; 9) appraisal of final image to allocate the 'undecided' class (if used) in initial classification; 10) creation of a mask to remove the mineral grains and pores to generate an image containing only the fine grained matrix; and finally, 11) the quantitative analysis of the clay matrix fabric.

Each of these steps, discussed more fully below, produces one or more intermediate images. To avoid confusion, all images are identified directly by a unique letter, so that the original BSE image is known as the *I - image*. A list of image labels is given in the Appendix.

Sample Preparation and Observation (stage 1, Fig. 5)

Samples were first impregnated with acetone and then with Araldite AY18 resin, as described in Smart and Tovey (1982). When hard, the samples were sawn with a diamond saw into blocks approximately 10mm x 10mm x 5 mm thick, polished with a 1µm diamond paste to form a flat surface, and coated with 20nm of carbon.

The samples were observed in the back-scattered electron mode in a Hitachi S450 SEM operating at 20kV. Contrast was adjusted so that the full dynamic range was achieved during digitisation on a 0-255 grey scale. While, visually, some BSE images appear better when the contrast is stretched so that the voids are suppressed to 0 on the grey scale and the brightest mineral is saturated at 255, it is important to avoid such saturation. Consequently, the images will show less contrast than is normal. Magnifications in the range x50 to x400 were selected for most observations. For detailed examinations of the clay matrix, magnifications up to x2000 were used. This range of magnification was chosen to show both the detail in the clay matrix and the distribution, size, shape, and orientation of the mineral grains.

All BSE images were digitised using a LINK Analytical AN10000 interface with a 512 x 512 pixel array. The magnification of the SEM was calibrated using a standard microscope grating and grid. At the nominal magnification of x1000, each pixel corresponded to 0.220µm. This calibration was essential for the particle size analysis included as part of this investigation. Many digitisation facilities and image processors use rectangular pixels. Square pixels were used throughout this work, which obviated the need for affine transformation of the images before analysis or, alternatively, the use of more complex algorithms (see Smart and Tovey, 1988, for example).

A general survey was made of the area covered by the BSE image to identify the key elements present using the energy dispersive X-ray system (EDS) attached to the microscope. In this particular sample, these elements included aluminium, silicon, sulphur, potassium, calcium, manganese, and iron. X-ray maps showing the distribution of these elements were acquired simultaneously together with a second BSE image, and the resulting composite image was also digitised. The EDS facilities available only permitted a spatial resolution of 128 x 128 pixels for any one elemental map. For this reason, the second BSE image, also at a resolution of 128 x 128 pixels, was acquired to check compatibility between the composite X-ray image and the BSE image. Both digital images from each area of each sample were converted into a format suitable for access by the image processing and analysis package.

The BSE image acquired at the same time as the X-ray maps was then magnified to the same size as the original BSE image using a bicubic interpolation routine. A check to ensure that both images were in register was then carried out using cross-correlation followed by a peak search to determine the location of the central maximum in the cross-correlation image. If this maximum did not correspond with the central origin of the original image, this indicated that a drift (either electronic or mechanical) had occurred within the SEM between the acquisition of the images, and the original image was translated accordingly. Rarely was the correction needed more than 1 pixel.

Mineral Segmentation (Stage 2, Fig. 5)

The BSE image and the composite X-ray image were displayed in the image processing and analysis package. Those X-ray maps which showed a distribution of a particular element across the area of interest were selected and extracted from the composite image. These were separately enlarged, as outlined above, to the same magnification as the BSE image and stacked in layers directly above it. Typically, 5 - 9 layers were stacked, depending on the mineralogy of the sample. The next part of the analysis, *mineral segmentation*, uses standard remote sensing techniques since the multi-spectral image that has been created is comparable to the several spectral bands of satellite images. Curran (1985) gives an introduction to the basic

classification techniques applied to satellite imagery.

The stacked image forms the basis for classification. First, a small irregular training area, typical of quartz, was defined using the computer mouse. The boundaries were defined and the co-ordinates specifying the region were stored. Other minerals were defined in a similar way. To aid in the delineation of the training areas, different layers of the stacked image were displayed on the screen as appropriate. Thus the quartz grains were most conveniently identified on the silicon X-ray map, while the relatively high concentration of potassium was used to identify the feldspar present. For the clay matrix, delineation of a typical area was best on the BSE image.

The various training areas may be analysed in the different layers to generate a co-variance matrix containing statistical information about the grey-level distribution in each layer of the stacked image for each class of mineral. It is desirable to minimize the number of layers in a stacked image. Thus, if iron and sulphur have a similar distribution, only one need be included. Tovey and Krinsley (1991) give a more complete description of the technique.

Once the covariance matrix has been computed, one of several classification procedures may be used. According to Tomlins (1981) the "maximum likelihood" classification method is the most accurate. It has been used in the research reported here, although it is more demanding on computing time than most other methods. During the classification, each pixel was coded to a value corresponding to the class in which it most likely fell. In the examples used here, the following class values were allocated:

class 1 - general clay/soil matrix
class 2 - quartz grains
class 3 - feldspar grains
class 4 - calcite/chalk grains
class 5 - iron oxide particles
class 6 - finely-ground calcite.

Provided that a correct selection of training areas has been made, classification proceeds smoothly. Normally, difficulties arise only if the classification covariance matrix is singular (see Tovey and Krinsley, 1991; Tovey et al, 1992c), and this only arises when there is no variation in contrast in one or more training areas in a particular layer of the stacked image. However, there are other aspects about which the user should be aware, even though this does not impede the classification. Standard classification routines frequently have an option to force classification at every pixel or, alternatively, to classify only if certain statistical criteria of probability are satisfied. (For instance, a class is allocated only provided that the grey-level values in the various layers at each pixel all lie within a given range of the mean values for that class and layer). The latter approach will lead to some areas of an image remaining unclassified (class 0).

Most of the *mineral-segmented* images generated (whether using a forced classification or not) usually require further processing quantitative work can be undertaken. In previous work, the authors mostly used a forced classification image as the starting point for this processing. Tovey and Krinsley (1991) investigated the variation in the results, in terms of mineral proportions, obtained using different methods for processing the raw images. They used both images in which classification was forced at each pixel and ones where differing amounts remained unclassified. Little difference in the results was noted provided that the results were weighted to normalise the area actually classified.

Part of Fig. 2 is used in this paper to illustrate the methods employed, and is shown in Fig. 6a. Figs. 6b to 6e show different aspects relating to the raw mineral-segmented images derived using multi-spectral methods. They are most conveniently viewed in false colour, but here the results are displayed in monochrome. In Fig. 6b, the initial multi-spectral analysis forced a classification at all pixels, while in Fig. 6c, a threshold criterion of 99% (corresponding to three standard deviations) was imposed. Several areas, coded black in this image, illustrate where classification in Fig. 6b could be potentially unreliable. Fig. 6d is derived from Fig. 6b and shows only those areas classified as feldspar (class 3). In this latter figure, those areas shown grey are classified as feldspar in both Fig. 6b, and 6c; those shown as white are only present in Fig. 6b, and may therefore, not be feldspar. Noticeable in Fig. 6d are fine (white) features surrounding the locations of the quartz grains. These are, almost certainly, artefacts and this emphasizes the importance of using care in the classification. For the method described in this paper, the image shown in Fig. 6c was used as the basis for further processing. For future reference, this raw classified image is referred to as the R - *image*. All mineral grains in both Figs. 6b and 6c appear to have holes in them. These holes mostly arise from topographic features on the surface and can be treated using standard hole filling routines. Fig. 6e shows the effects of this 'hole filling' to generate the R^h - *image*.

Treatment of Large Voids (Stage 3, Fig. 5)

Large voids and channels (> 0,01mm wide) appear as the darkest regions in the images. There is little or no variation in grey level across these regions and, if training areas are selected within these, the resulting covariance matrix is often singular. As the large voids are generally well defined, objective techniques to segment an image by thresholding may be used to define accurately the regions covered by such voids (e.g. the weighted relative contrast method developed by Kohler (1981) and adapted for porosity analysis by Hounslow and Tovey, 1992). This method generates a multi-modal histogram in which the peaks define the optimum values for choice of a threshold. In a two-phase material, the histogram is unimodal. In real soils, several peaks are present, corresponding to the different component phases. Fig. 7a shows the relative contrast histogram derived from Fig. 6a. There are 3 separate peaks, and it is usually a simple matter to assess which of these maxima should be chosen for the threshold level to generate a binary image to define the pores (the P - *image* as shown in Fig. 7b). When combined with the R^h - *image* (Fig. 6e), this P - *image* produces the R^p - *image* which can be further modified by removal of the matrix to leave only the large mineral grains as R^* - *image* (Fig. 7c). For some purposes, later in the process, a binary version of R^* is needed; this is termed the R^b - *image*. At this point, stages 1 to 3 (Fig. 5) in the processing have been completed.

Definition of Particle Shapes (Stages 4 and 5; Fig. 5)

The R^* - *image* remains unsatisfactory for quantitative work because the edges of the mineral grains are ill defined and bear little resemblance to the 'real' edges as shown in the original BSE image (the I - *image* -see Fig. 6a). Information from edge detection routines on the I - *image* could be used to define the edges more effectively. Accordingly, the magnitude of the intensity gradient vector was computed at each pixel in the I - *image* using a fourth order least squares formula (Smart and Tovey, 1988). This algorithm is summarized in Tovey et al. (1992) and uses 20 points in a circular array around each pixel and is, thus, more robust than simple detection routines (e.g. the Roberts and Sobel operators) that use only the nearest pixels. The resulting magnitude image (M - *image*) is shown in Fig. 8a where several of the edges of the grains are well defined. It is now
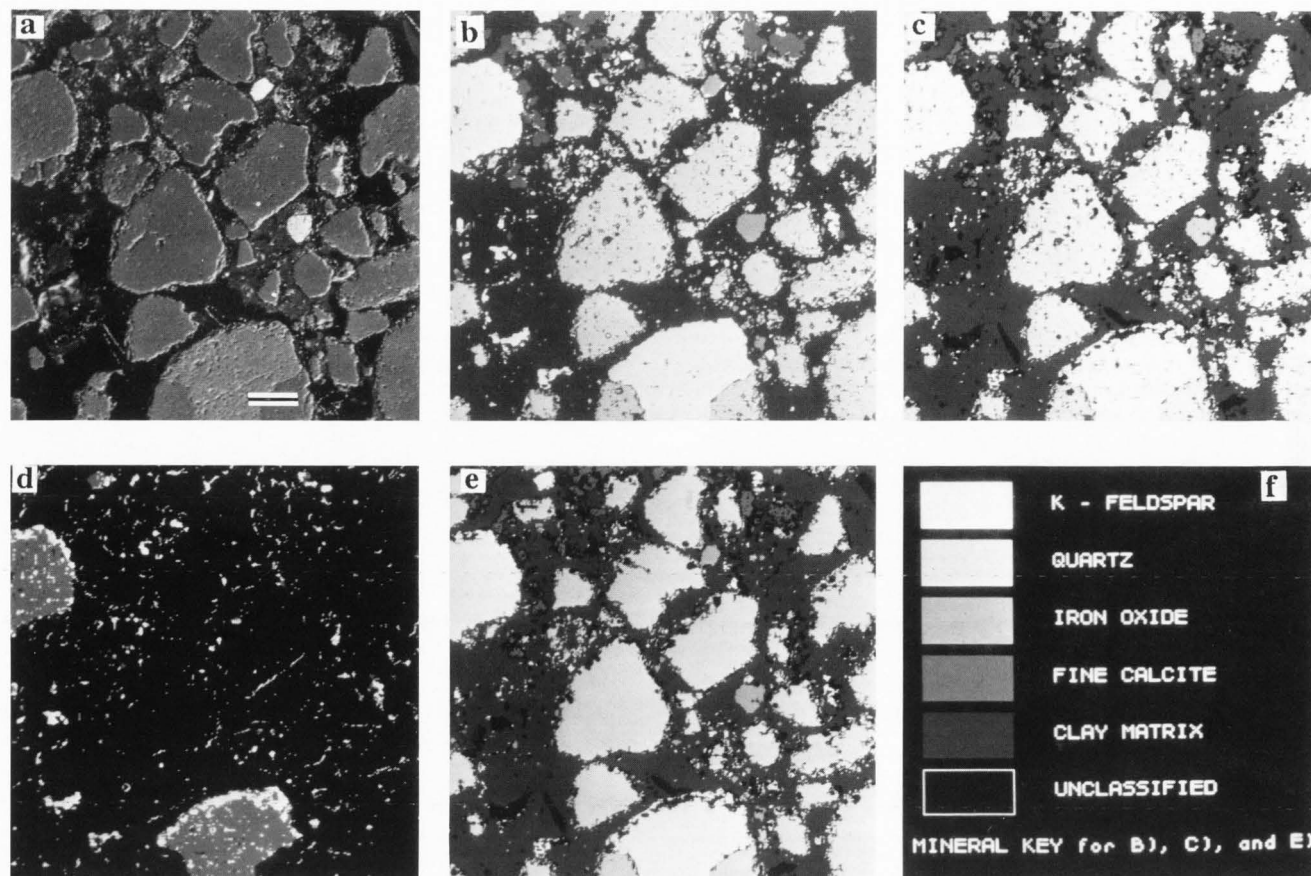
Fig. 6. Images of basic classification: a) BSE image, b) forced classification at all points; c) classification allowing some uncertainty (**R - image**); d) difference in (b) and (c) in connection with feldspar grains; e) **R^h - image** generated by filling holes in **R - image**; f) key to minerals in (b), (c) and (e). Bar = 0.1 mm.
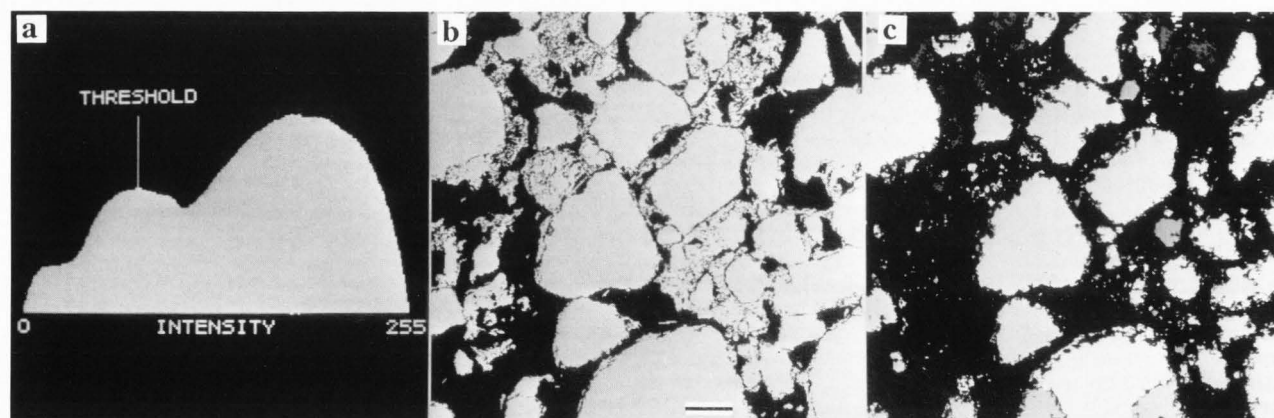

Fig. 7. Generation of porosity image: a) relative contrast histogram of Fig. 6a; b) **P - image** using information from (a) and **I - image** (Fig. 6a); c) the **R* - image** obtained by combining the **R^h - image** (Fig. 6e) with (b). Bar = 0.1 mm.

necessary to select a threshold value which defines all edges and which does not over-segment the image. After much empirical experimentation, it has been found that a threshold set at 10% of the maximum magnitude level defines all the mineral grains. However, some grains, such as the feldspar grain at the bottom centre, have several edge lines within the grain. These over-segmentation lines arise from the contrast associated with the pitting on the surface of some grains (Fig. 8b). Some of these redundant lines may be removed by eroding Fig. 8b to generate a skeleton image, followed by the
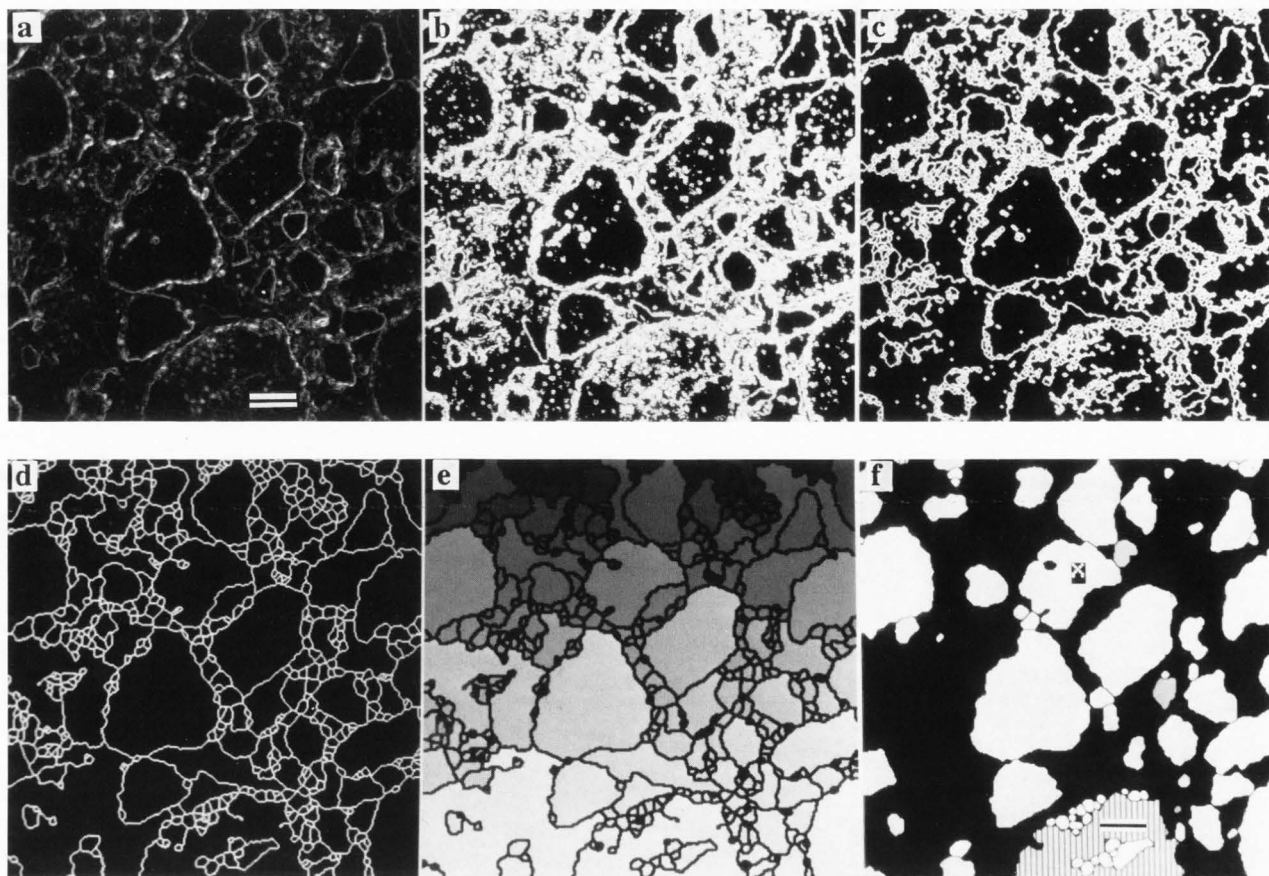
274

Fig. 8. Stage 6 of the process: a) magnitude image; b) binary image of (a) thresholded at 10% level; c) skeletal image of (b); d) further skeletal image after one dilation/erosion cycle; e) identification of each feature area; f) Improved classification image (U_o - image) generated through use of the transform matrix (T - image). The shaded grains are those automatically identified as multi-mineral grains; the grain labelled X requires further treatment to remove the hole. Bar = 0.1 mm.

removal of the disconnected ends in the skeletal network. This still leaves an image that is very confused (Fig. 8c; the S - image). The situation is further improved by a dilation followed by a second erosion combination to produce Fig. 8d (S^* - image). While this still contains unnecessary detail in terms of lines within grains, it does include the key edges of the mineral grains.

It is now a simple matter to identify each area in Fig. 8d, using standard feature analysis facilities, shading each area with an unique intensity value (Fig. 8e). This is called the feature image (F - image). To reduce unnecessary detail, features which covered less than 5 square pixels (i.e. were of clay size) were omitted in this stage (the information from these small areas is reinserted at a later stage). Some of the areas in Fig. 8d clearly represent mineral grains (or parts of mineral grains if there has been over-segmentation), others relate to voids or the clay matrix. Some of the mineral grains have holes within them (e.g. 'X' in Fig. 8d).

Allocation of Mineral Grain Classes (Stage 6, Fig. 5)

A matrix to transform the data to remove this oversegmentation (called the T - image) is now constructed which has as many columns as there are features in Fig. 8e (1 to 459 in this case). The number of rows depends on the number (n) of mineral species present. There is one row for
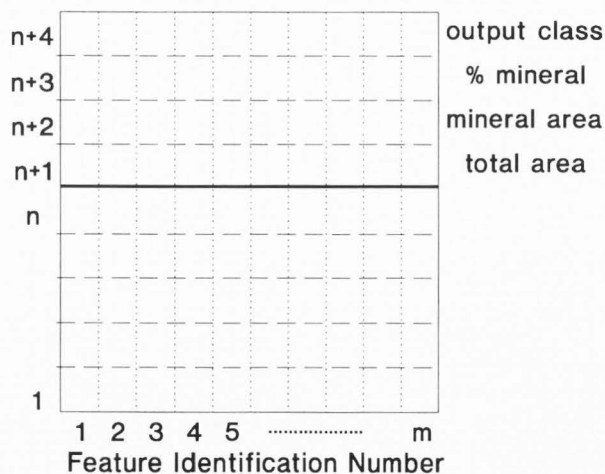

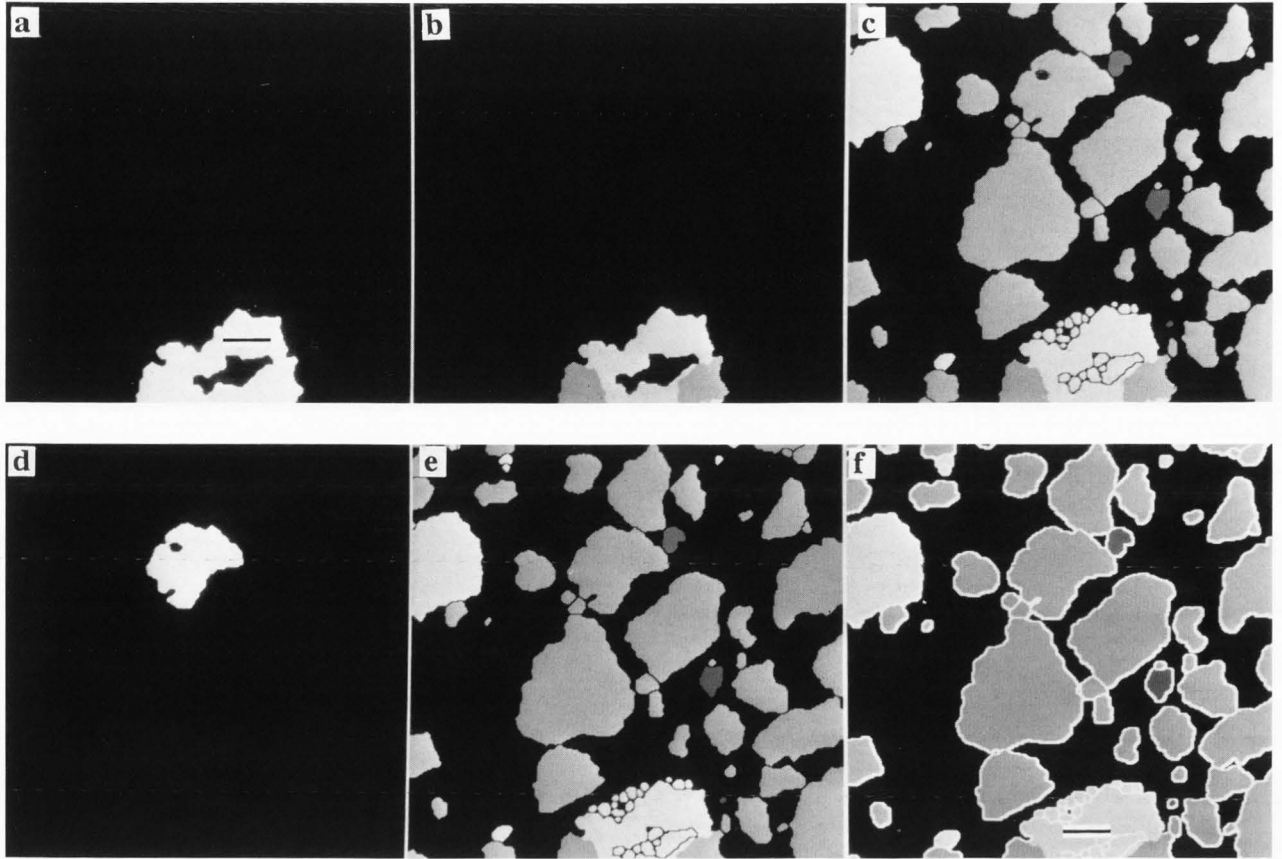Fig. 9 Schematic representation of the transform matrix (T - image).

Fig. 10. Treatment of multi-mineral grains: a) definition of areas of such grains; b) dilation of R^* - image within these areas; c) combination of (b) with U_o - image; d) identification of grains with holes; e) combination of (c) with (d) after hole filling; f) outline of features using edge detection (V_2 - image). Bar = 0.1 mm.

each selected mineral. However, it is convenient to have four extra rows for working space in the matrix. Fig. 9 graphically illustrates the layout of the T - image.

Rows 1 to n will contain information on each mineral species, while rows n + 1 to n + 4 are used as working space. The coefficients in rows 1 to n+1 are then determined as follows:

1) For each mineral type, a temporary new image is generated by setting each pixel value equal to the corresponding one in the F - image if the associated pixel in the R^* - image is a member of the selected mineral class, otherwise the pixel value is set to zero. Thus a new set of images, denoted A_1 .... A_n is produced, one image for each of the n mineral classes present.

2) Histograms H_1 .... H_n showing the frequency of occurrence of each of the intensity values in the images A_1 to A_n are computed, care being taken to ensure that all the histograms cover the full range as specified in the F - image.

3) The values in the in the rth row of the T - image are then filled with the values in the corresponding position in H_r.

4) A further histogram H_t is computed showing the total frequency of occurrence of the intensity values in the F - image. The values in H_t are then copied into the corresponding positions in the $n+1^{th}$ row of the T - image.

The rows n+2 and n+3 in the T - image are computed from the rows 1 to n+1 as follows:-

Row n+2
$$T_{n+2,i} = \sum_{r=1}^n T_{r,i} \quad (1)$$

where i is the identification value from the original F - image.

Thus $T_{n+2,i}$ represents the total area (in pixels) of the feature in the F - image covered by classified minerals. This area will generally be less than the value $T_{n+1,i}$ since the latter covers the total area of each feature.

Row n+3
$$T_{n+3,i} = T_{n+2,i} / T_{n+1,i} \quad (2)$$

i.e. $T_{n+3,i}$ represents the proportion of the ith feature covered by mineral grains.

At this stage, it is convenient to normalise the values in rows 1 to n in the T - image as follows:-

$$T_{r,i} = T_{r,i} / T_{n+2,i} \quad (3)$$

This equation follows the computer notation to replace the new value of $T_{r,i}$ with the old value expressed as a percentage of the total area covered by mineral grains in each feature.
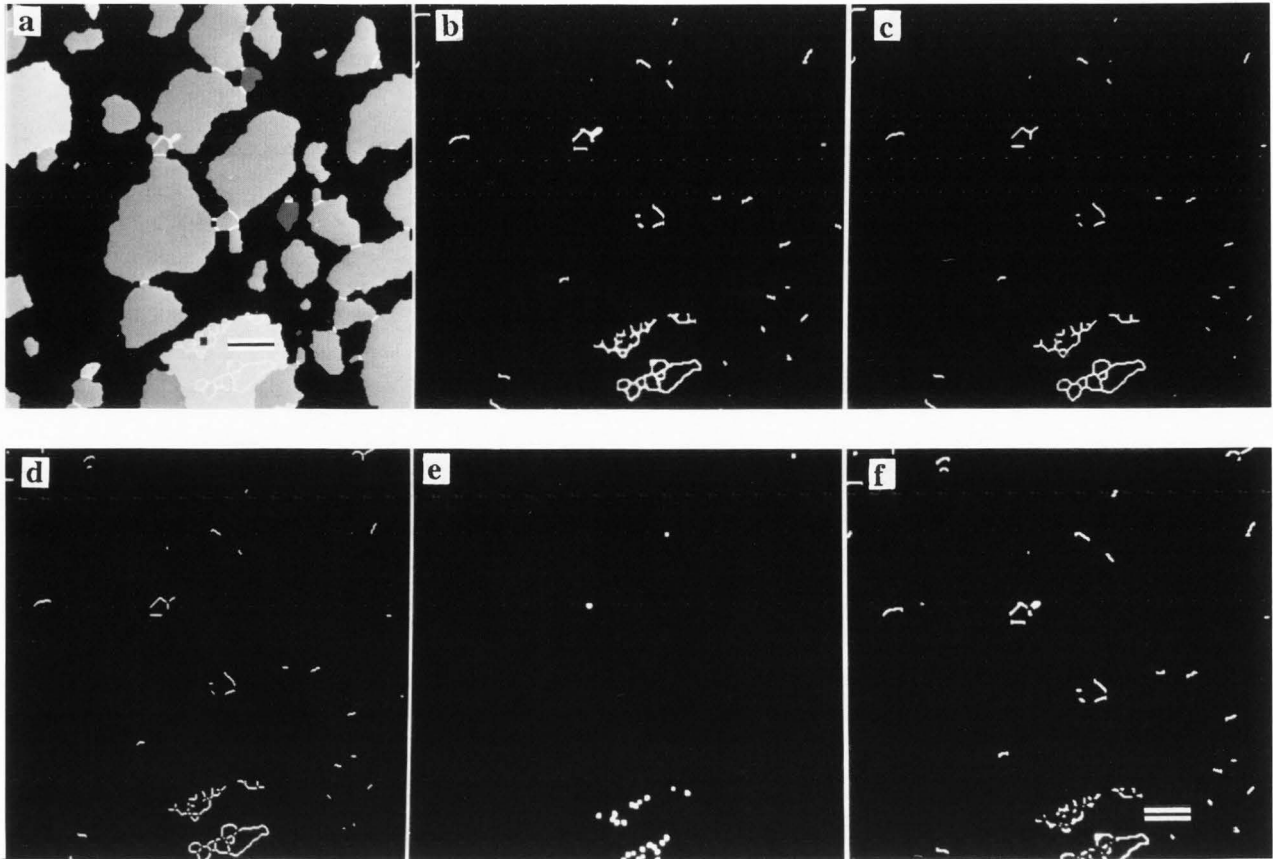
276

Fig. 11. Sequence used to remove over-segmentation lines: a) V_2 - image eroded to leave grains and over-segmentation lines and lines between grains; b) after removal of mineral grains;c) skeletal lines; d) erosion of nodes; e) dilation of nodes; f) removal of node areas in (e) from (b).   Bar = 0.1 mm.

The final row (n+4) of the T - image is then used to specify a classification type for each of the features in the F - image. Three different criteria must be established:

1) Features with low total percentage of mineral grain, as shown by the value in $T_{n+3,i}$, are not classified and, accordingly, a value of zero is recorded for $T_{n+4,i}$ A threshold value t_m must be selected to separate those areas to be classified as mineral from those which are not. The value of t_m will depend on the exact method of classification used in the original R - image. In the work reported here, a value of 0.20 was used, but some further experimentation would seem desirable (see the discussion).

2) Features are classified according to the dominant class, i.e. the maximum of the values $T_{1,i}$ to $T_{n,i}$. Normally, only one class is present, but occasionally, there are features in the F - image which contain a second mineral in significant proportions. Provided that the second most dominant mineral in any feature was present in quantities less than 5%, the value $T_{n+4,i}$ was coded to the class value of the dominant mineral.

3) Features which have two or more minerals in significant quantities (i.e. >5%) were coded to an out of range value (99 in this case) for subsequent alternative treatment.

It is a simple matter to modify the values in the F - image according to the values in row n+4 of the T - image. This produces another intermediate image, called the U_0 - image, which has used the correct outlines from the S - image to define the extent of the mineral grains, and completes stage 6 of Fig. 5. The U_0 - image is shown as Fig. 8f. There remain four residual problems which must be addressed before the final classified image can be obtained. These are:

1) Problems associated with multi-mineral grains (coded 99 in the U_0 - image);
2) Holes in particles in the final image arising from holes in the F - image;
3) Over-segmentation;
4) Unclassified areas in the R^* - image which adjoin the mineral grains.

Treatment of Multi-Mineral Grains (Stage 7, Fig. 5)

The first of these difficulties is readily overcome by generating a new image (V_0 - image). The features classified by the out of range value (99) in the U_0 - image define the full spatial extent of the multi-mineral grains, and these are copied to the V_0 - image which is then scaled to form a binary image which has values of unity, where there are the multi-mineral features, and zero elsewhere (Fig. 10a). A new image V_1 is first computed as:
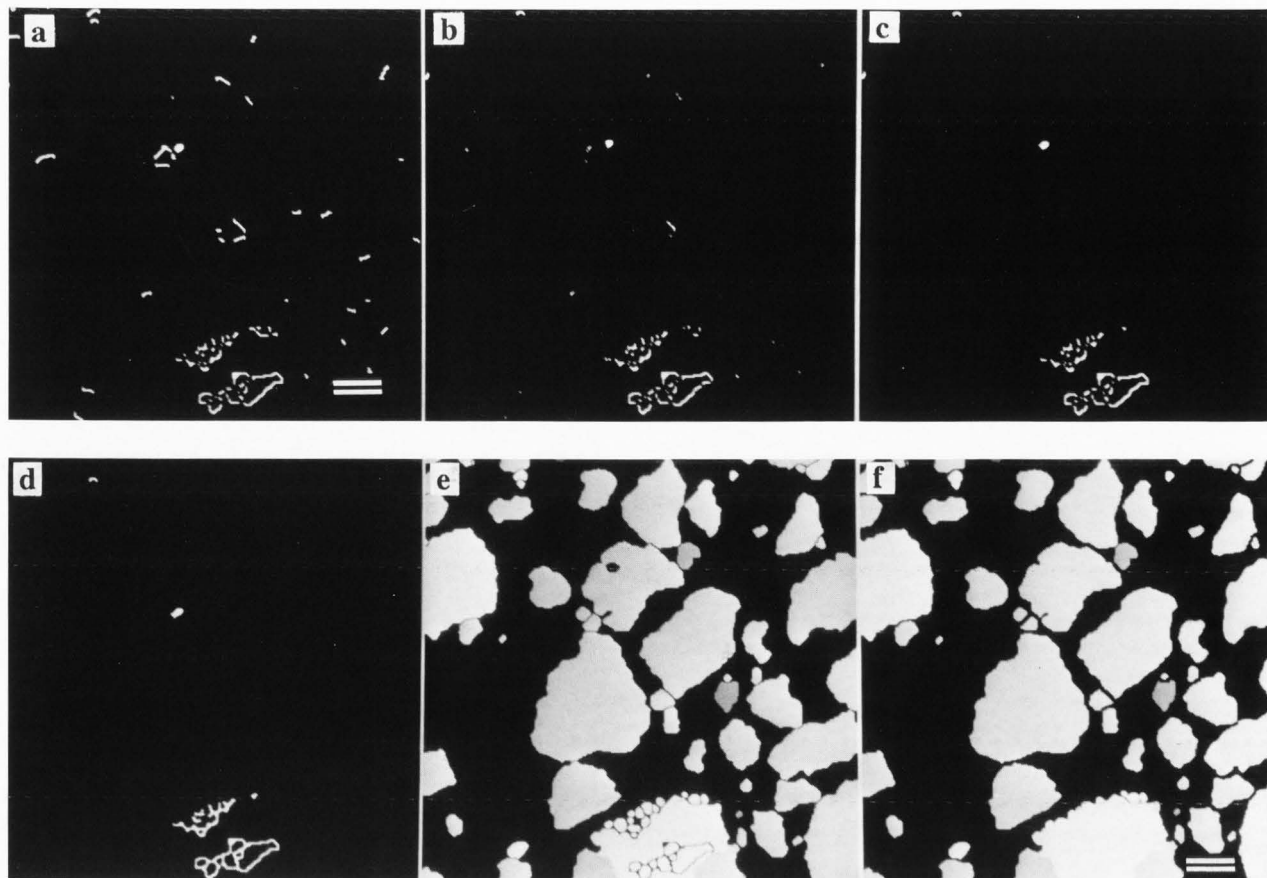
$$V_1 = V_0 . R^*$$ (4)

277

Fig. 12. Completion of over-segmentation removal: a) identification of lines; b) combination of (a) with R^* - **image**; c) after analysis with ratio histogram (H_3^*) to locate only over-segmentation lines; d) dilation of (c) to fill areas covered in Fig. 11b which is combined with the U_o - **image** in (e) to produce (f) where all the over-segmentation lines have been removed but leaving the lines delineating separation between grains.   Bar = 0.1 mm.

then the mineral areas in V_1 are dilated to fill the regions defined by V_0 (Fig. 10b), care being taken to ensure that the different mineral species do not dilate over one another. The V_1 - **image** is now pasted onto the U_0 - **image** to generate the U_1 - **image** (Fig. 10c), which resolves the first difficulty.

Removal of Holes/Treatment of Over-Segmentation

Most image analysers have facilities to remove holes within features, either directly or through intermediate stages. In the example used, one such feature had a hole (marked 'X' in Fig. 8d). Removing such holes resolves the difficulty (2) above to generate the U_2 - **image** (Fig. 10e).

It is clear that the large feldspar grain at the bottom centre of Fig. 10e is over-segmented. Several steps are needed to resolve this problem. It is convenient to start by generating a new outline image (the E - **image**). Since the edges are now sharply defined, a simple edge detection routine may be used (e.g. the Roberts edge detector). The E - **image** is dilated to thicken the lines (this ensures that all the lines between features are filled) to form the E^* - **image**. This image and the U_2 - **image** are combined to form the V_2 - **image** (Fig. 10f) which will have have features which are larger than the correct size by 2 pixels. These edge lines are of three types:- 1) outside boundaries of the grains; 2) boundaries between grains, and 3) the over-segmentation

lines. A double erosion of V_2 produces the V_3 - **image** (Fig. 11a) in which the boundary lines have been removed. It is now necessary to distinguish between the over-segmentation lines and those correctly marking the boundaries between features. Processing proceeds by obtaining just these lines (Fig. 11b), skeletonizing the outlines (Fig. 11c), and then eroding the nodes to disconnect the various lines from one another (Fig. 11d). The sites of the nodes are dilated (Fig. 11e) and this image is used to separate the original lines from Fig. 11b as Fig. 11f. This latter image thus has a collection of short, disconnected lines.

Fig. 11f (the V_4 - **image**) is also displayed as Fig. 12a except, at this stage, each line is given an unique identifier. A histogram H_1^* of V_4^* is computed except that the zero class representing the background is omitted. H_1^* stores information on the area of each of the lines (the term area is used as some lines are thicker than one pixel). Proceeding as follows:

$$V_5 \qquad = \qquad V_4^* . R^b \qquad (5)$$

generates a new image (Fig. 12b) which has intensity values in the same range as V_4^* but the areas of some lines will be reduced as they partly cover the gaps between particles as defined in the R^b - **image**. A histogram H_2^* is computed of the values in V_5, and a new one-dimensional image H_3^* is
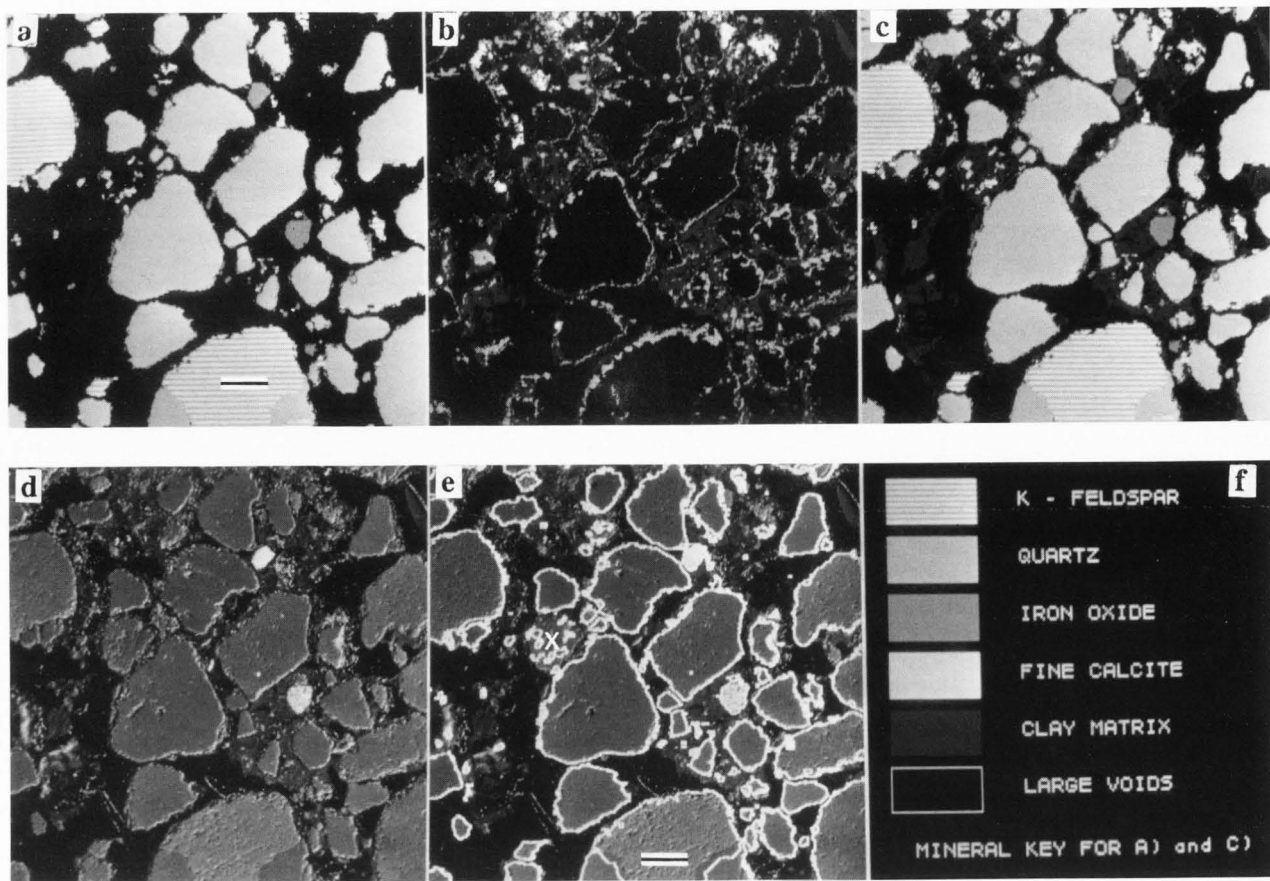
Fig. 13. Final images: a) image **V₆ - image** obtained after dilation of mineral grains into peripheral unclassified regions; b) full extent of all unclassified regions; c) final image (**Z - image**) after classifying residual uncertain areas as clay matrix; d) original image for comparison; e) original image overlain by edges of grains from (c); f) mineral key for (a) and (c). Bar = 0.1 mm.

now computed as:

$$H_3^* = H_2^*/H_1^* \qquad (6).$$

The H_3^* - *image* contains the percentage of each line identfied in the V_4^* - *image* which remains in the V_5 - *image*; those with a low percentage are features which mark the boundaries between grains, those with a high or 100% value are, clearly, lines lying entirely within grains and are thus the over-segmentation lines. Image V_6 (Fig. 12c) is generated by the selection of a threshold (t_s) to retain only those lines with a high percentage value in H_3^*. The complementary image (V_6^*) is also generated at this time, showing only the lines separating grains. In this work, a value of 70% was chosen for t_s. While there is scope to consider the exact choice of value, some experimentation did show that there was little or no change in the final result, even with quite large changes in t_s. It is important to make the distinction between the two types of line, as those not associated with oversegmentation need to be retained to separate touching features.

Fig. 12c is now dilated to fill the gaps created by the nodes and combined with the V_4 - *image* to produce Fig. 12d. This figure only displays the oversegmentation lines. It is now a simple matter to dilate the U_2 - *image* (Fig. 12e) to fill the intergrain spaces, and then to add information from the V_6^* - *image* which contains information about grain
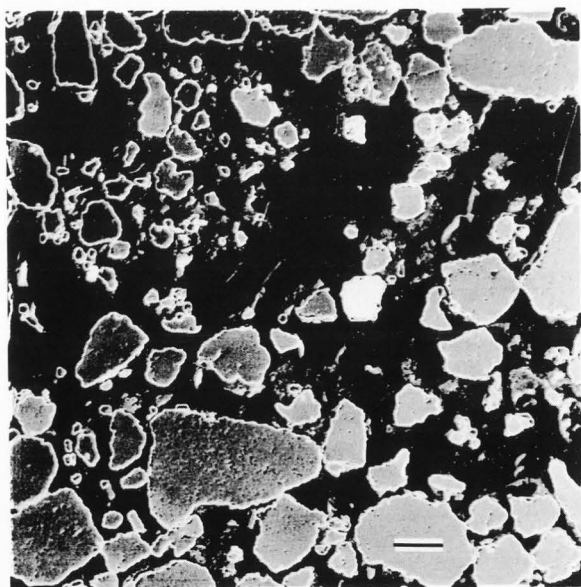

Fig. 14. Another example of a BSE image showing the overlaying of the final edges as determined in the procedure outlined above. Bar = 0.1 mm.

279

separation, to produce image U_3 (Fig. 12f), in which over-segmentation has been removed. There is, sometimes, a minor residual problem in that the occasional hole remains in the mineral grains between the original features after removal of the over-segmentation lines (e.g. the feldspar at the bottom centre of Fig. 12e). Standard hole filling routines may be used if required (Fig. 12f).

Treatment of Unclassified Areas (Stage 9, Fig. 5)

The final difficulty is to deal with unclassified areas at the boundaries to the mineral grains. The U_3 - image is combined with the unclassified regions from the modified raw classified image (R^h -image - Fig. 6e) to give the U_4 - image. Some of these regions lie adjacent to the edges of the mineral grains, and one reason for their presence is the slight highlighting of the edge of many grains in the I - image. In the absence of conflicting information, the best way to deal with the unclassified areas immediately adjacent to the grains is to dilate the mineral grains only into these regions, as shown by the U_5 - image (Fig. 13a) - the full extent of the unclassified regions is shown in Fig. 13b. It will be noted that those unclassified areas immediately adjoining the mineral grains have already been incorporated into Fig. 13a. The U_5 - image has the outlines of the mineral grains and it remains to reinsert the information for the matrix, pores and other unclassified areas from to form the U_6 - image as follows:

$$U_6 = U_5 + (R^p - R^*) \qquad (7)$$

All the fine grained material is now incorporated, and the final step is to allocate the remaining unclassified regions. These all lie within the clay matrix and it would seem logical to include them as such. The final image in this post-processing (the Z - image) is shown as Fig. 13c. For comparison, the original image is shown as Fig. 13d together with a combination image showing the final computed outlines of the grains (Fig. 13e).

Discussion and Applications

The example used to illustrate the procedure proved to be more difficult to process than most. Most images can be treated more simply. Thus Fig. 14 shows a further BSE image of the same sample, once again with the final grain outlines highlighted. This time, however, there was no problem from holes within grains or from over-segmentation.

The final image from (Fig. 13e) does show some areas which warrant discussion. Thus the grain at 'X' does not appear to have been included in the initial mineral classification and is coded as clay mineral. Close examination of all the X-ray maps did indicate that it bore no resemblance to any of the other mineral species identified and, in terms of the aluminium and silicon concentrations (the only elements present in significant quantities), the proportions were very similar to that of the clay matrix. It is not surprising that the image analysis has coded this grain accordingly. Even subjectively, the operator could not differentiate the area from the clay mineral except in terms of the morphology in the BSE image. After classification as described above, the sample was re-examined in the SEM. At high magnification, the morphology did, indeed, suggest that the area was predominantly clay mineral.

Stages 3 - 9 (Fig. 5) of the procedure may be completed without operator intervention, which satisfies the initial requirement that it should be both objective and suitable for batch processing. The Z - image is in an ideal form to generate a binary mask of the mineral grains and voids (step 10 in Fig. 5) so that only the clay matrix regions are displayed, as in Fig. 1b. Equally, the Z - image may be used to quantify the particle size distribution and the shape and orientation of the separate mineral grains; something which cannot be achieved by other methods. Images such as Fig. 1b may be used to study the orientation of the fine grain features since, when large grains are present, the quantitative estimates of orientation are often distorted. Intensity gradient methods may be used to estimate the degree of orientation within this clay matrix, while domain segmentation methods can segment the image to show regions of different orientation. In Fig. 1c, it is clear that the clay matrix has flowed around the larger grains: in other soil samples, this has not been the case (Tovey et al. 1992c).

While the method can be used in batch mode without operator intervention, a few key parameters must be chosen at the outset. These are 1) the exact threshold value used to generate the binary image from the magnitude image (a value of 10% maximum value was used here); 2) the threshold proportion of each feature covered by mineral grains (t_m - chosen as 25% in this example); 3) the percentage above which a second mineral becomes significant (set at the 5% level in this example); and 4) the threshold level used in the segregation of true lines of separation from the over-segmentation lines (t_s - 70% in this example). There is scope for investigating the effect of choice of these parameters on the overall result. However, a brief consideration of the last of these parameters showed no change in the final result if the threshold value was reduce by 20% to 50%, and it would appear that the exact choice is not critical.

Acknowledgements

References

Curran PJ, (1985). Principals of Remote Sensing, Longman, London, Chapters 2 - 4.

Ehrlich R, Crabtree SJ, Kennedy SK, and Cannon RL, (1984). Petrographic image analysis, I. Analysis of Reservoir Pore Complexes. Journal of Sedimentary Petrology, 54: 1365-1378.

Foster RH and Evans JS, (1971). Image analysis of clay fabric by Quantimet. The Microscope, 19: 377-401.

Hounslow MW and Tovey NK (1992). Porosity Measurement and Domain-Segmentation of Back-scattered SEM Images of Particulate Materials. Scanning Miscrosc. Supplement 6, 245 - 254.

Kohler R, (1981). A segmentation system based on thresholding. Computer Graphics and Image Processing. 15: 319-338.

Lafeber D, (1967). The optical determination of spatial (three-dimensional) orientation of platy clay minerals in soil thin sections. Geoderma, 1: 359- 369.

Morgenstern NR and Tchalenko JS, (1967a). The optical determination of preferred orientation in clays and its application to the study of microstructure in consolidated Kaolin I. Proc. Royal Society, Series A., 350: 218-234.

Morgenstern NR and Tchalenko JS, (1967b). The optical determination of preferred orientation in clays and its application to the study of microstructure in consolidated Kaolin II. Proc. Royal Society, Series A., 350: 235-250.

Protz R, Sweeney SJ, and Fox CA, (1992). An application of spectral image analysis to soil micromorphology. Geoderma, 53: 275-288.

Smart P and Tovey NK, (1982). Electron microscopy of soil and sediments: Techniques. Oxford University Press, Oxford, chapters 4,5 and 10.

Smart P and Tovey NK, (1988). Theoretical Aspects of Intensity Gradient Analysis. Scanning, 10: 115-121.

Tchalenko JS, Burnett AD, and Hung JJ, (1971). The correspondence between optical and x-ray measurements of particle orientation in clays. Clay Minerals, 9: 47-70.

Tomlins GF, (1981). Canadian experience in wetland monitoring by satellite. In: Smith, H. (Editor), Plants and the Daylight Spectrum. Academic Press, London, 102-113.

Tovey NK, (1973a). A general photogrammetric technique for the analysis of scanning electron micrographs. Proceedings: SEM Conference, Systems and Applications, Institute of Physics, London, 82-87.

Tovey NK, (1973b). Quantitative analysis of electron micrographs of soil structure. Proceedings of International Symposium on Soil Structure, Gothenburg, Swedish Geotechnical Society, Stockholm, 50-57.

Tovey NK and Wong KY, (1978). Optical techniques for analysing scanning electron micrographs. Scanning Electron Microsc. 1978;I: 393-400.

Tovey NK, Smart P, Hounslow MW, and Leng XL, (1989). Practical Aspects of Automatic Orientation Analysis of Micrographs. Scanning Microsc: 3(3): 771-784.

Tovey NK and Krinsley DH, (1991). Mineralogical mapping of scanning electron micrographs. Sedimentary Geology, 75: 109-123.

Tovey NK and Krinsley DH, (1992). Mapping the orientation of fine-grained minerals in soils and sediments. Bulletin of the International Association of Engineering Geologists, 46: 143-157.

Tovey NK, Smart P, Hounslow MW, and Leng XL, (1992a). Automatic domain mapping of certain types of soil fabric. Geoderma, 53: 179-200.

Tovey NK, Smart P, Hounslow MW, and Desty JP, (1992b). Automatic Orientation Analysis of Microfabric. Scanning Microsc. Supplement 6, 315-330.

Tovey NK, Krinsley DH, Dent DL, and Corbett WM, (1992c). Techniques to Quantitatively Study the Microfabric of Soils. Geoderma, 53: 217 - 235.

Appendix

List of Images Used In Procedure

$A_1....A_n$ Intermediate images used in the construction of the *T - image*.

B   Binary image to mask the large mineral grains and voids to create an image for domain segmentation of fine grained matrix.

D   Domain segmented image

E   Image defining edges derived towards end of process and used in the removal of over-segmentation lines.

F   Image generated from segmented *S - image* in which each feature is identified by an unique grey level value

$H_1....H_n$ Histograms derived from A_1 to A_n.
$H_1^*...H_3^*$ Histograms associated with removal of over-segmentation lines.

I   Original BSE image.

M   Magnitude of intensity gradient vectors of *I - image*.

O   Orientation image of intensity gradient vectors of *I - image*.

P   Binary image generated from the *I - image* showing porosity derived using a weighted relative contrast method to determine the correct threshold level.

R   Basic raw classification image. The image may incorporate unclassified regions depending on parameters selected during classification.

R^h Raw classification image modified to fill holes in mineral grains.

R^p R^h - *image* modified to incorporate porosity information from *P - image*.

R^* R^p - *image* modified by removal of matrix to leave only large mineral grains.

S   Skeletonized image derived from *M - image*.

T   Transformation matrix used to assign classification to each of the features in the *F - image*.

$U_0 - U_n$ Intermediate images used in last stages of procedure.

$V_0 - V_n$ Further intermediate images used in calculation.

X_r X - ray map images; the subscript **r** (if used) refers to the element number.

Z   Final classified image suitable for final quantitative analysis or transformation using the *B - image*.

Discussion with Reviewers

G. Bonifazi: In the "maximum likelihood" classification method, a preliminary classification of the informative content of each layer (X-ray maps) has to be realized. The authors clearly remark this aspect, but no mention is reported about the fact that, differently from the image usually derived from remote sensed data (e.g. Landsat), where this classification procedure is widely used, in the case of X-ray maps we have, on each plane, a discrete set of information (counts) related to the element content analysed and detected. Have the authors encountered problems, during the preliminary stage of the studies, due to this fact? Do the authors think that a further preliminary processing of X-ray maps, in order to reduce the absence of information between a count and another, could ameliorate the procedure discussed?

Authors: We have encountered no significant problems here. Some pre-processing has been tried (e.g. thresholding), but often this has created more problems than it has solved (Tovey and Krinsley, 1991). In other cases, we tried various forms of filtering, but these changed the final results very little. The most serious problem is the difficulty over boundary regions. It is possible to force a classification, but then unlikely classes are attributed to these regions. It is better to leave these unclassified initially, and use information from the BSE image to define the true extent of each grain. Whatever pre-processing is done, this last problem will always remain, and it is to this end that this paper is directed.

Reviewer 2: Referring to Fig. 10b, it is stated that care is taken to ensure than the different areas do not dilate over one another. What test is used to check this?

Authors: We use a grey-level dilation, and continue successive dilations until the gaps *within the relevant grain* and between the different mineral areas just merge.

Reviewer 2: How are the figures 3a and 3b obtained? There is not an obvious relation between Figs. 2, 3a and 4. The grey-scale of the histogram is not directly related to one particular class?

Authors: Figs. 3a and 3b were included to highlight the problem to which the Reviewer refers. Indeed, it is not possible to differentiate, on the BSE grey-scale values alone,

between the two mineral species. In actual practice, as indicated in the text, Figs. 3a and 3b can only be obtained once the full procedure described in the paper has been completed. To obtain the histograms, Figs. 3a and 3b were derived from the final image *Z - image* (Fig. 13c). The separate areas were then masked, and histograms were computed separately for the quartz and feldspar.

Reviewer 2: It is stated that Fig. 1 shows that the matrix is highly aligned. It seems to me that this is a little too strong a statement: the effect of alignment could result, in part, from the method of preparation. This statement ought to be reviewed.
Authors: Orientated clay layers form as cutans around larger silt and sand grains and have been widely reported in the literature. In other soils, see for instance the Blacktoft Series image shown by Tovey et al. (1992c), there is no evidence of any alignment. It thus seems that this is a genuine effect, and not as suggested, a problem with preparation.

J. Bonifazi: The authors correctly affirm that the techniques illustrated in the paper, developed for a two-dimensional domain, can easily be extended to three-dimensions following a modified procedure based on a certain number of observations on "orthogonal planes in each sample". Every time a procedure to analyse and characterize particles or grains by image processing is developed, the problem to extend the results derived from bi-dimensional analysis to three-dimensional space represents the main question arising at conferences, seminars, symposia or review works. I think that, from a practical point of view, this is not a real problem for two types of reason: a) the analyses are generally carried out automatically, as in the case of this work, so a great number of samples can be processed and a great number of connected domains analysed; b) even if we could have the possibility to realize "direct" or "indirect" 3D investigations, the computational, in the first case, and the reconstruction and computational problems, in the second case, could largely defeat the effort to develop a software architecture, compared to those based on image processing techniques, which are useful and easy to use, as those described in the paper. What do the authors "really" think about this?
Authors: We agree that the 3D problems are often grossly over-stated, often by those who are critical of image analysis methods. In one instance we do consider the three-dimensional situation. The overall *resultant* vector specifying the preferred orientation of all the fine-grained particles is the two dimensional projection of what is, in reality, a 3D vector. It is possible to combine observations from other planes to obtain the true spatial orientation of this vector. In theory, this vector, can then be related to the stress tensor, and this is our ultimate aim, but one which we have yet to complete.

J. Bonifazi: Describing the "sample preparation and observation", the authors reported that the BSE images of the sample were acquired twice, at 512 x 512 pixel resolution and at 128 x 128 pixel resolution, the lower resolution was used to check compatibility with the elemental maps. A bicubic interpolation and a registration procedure were then applied in order to produce sample images (X-ray maps) at 512 x 512 pixels. In the paper, there is no mention about the fact that an interpolated (magnified) image presents a Fourier power spectrum different from the original one. Generally, the interpolated image presents a low high frequency content in the Fourier domain if compared with the source image. Have the authors considered this aspect? Why have the authors chosen a bicubic and not, for example, a linear or bicubic B-spline interpolation?
Authors: Yes, we are aware of the Fourier problem but we did not consider it serious since the X-ray maps are noisy

anyway. With regard to other interpolations, we did also try bi-linear interpolation and found that the ultimate results, after all analysis, were almost indistinguishable from those using bicubic interpolation. We considered the problem to be of low priority in our current work. Indeed, in the last few months, we have been able to acquire the X-ray maps directly at the same resolution as the BSE images.

Reviewer 2: It is not evident that a 'hole' exists in Fig. 6a. This may arise from the global treatment of the gradient image. Perhaps a local operator could be used?
Authors: The hole does arise from the textural surface details on the particular grain, something which is not that uncommon. A local operator could perhaps be used, but we are satisfied that we can deal with the problem of 'holes' in the manner outlined.

F. Grillon: Have you quantitative results on your procedure? What is the precision of the results?
Authors: Two preliminary sets of quantitative data were presented in Tovey and Krinsley (1991), and Tovey et al. (1992c). It would be necessary to study many more images before a statement on the precision of the results can be given.

F. Grillon: Do you know the Image Acquisition and Processing program of Tracor Northern which was on the market before 1980? It made on line multi-spectral measurements.
Authors: Tracor Northern were not the only one to have such packages (e.g. Link Analytical). The main difference between those packages and the procedure reported here is that we use the higher resolution inherently achievable from the BSE image and combine it with the lower resolution information from the X-ray maps. We also do not require that the various X-ray maps be separately thresholded as some packages require.

J.A. Swift: A most elegant piece of work. The methods here are clearly designed to eliminate operator influences over the results. To what extent are the working image fields selected without operator bias, and if so, how have you gone about this? It would also be useful if you could indicate the time taken, and the number of samples needed, to find out what you want to know about the typical sample, and the cost in dollars.
Authors: The selection of image field is clearly a fundamental problem. The work in this area has been directed to solving the image processing problems, and we are aware of the operator bias difficulty at the time of image acquisition. In other related work (Tovey et al. 1992a,b), it is our normal practice to take 24 or more images on a regularly spaced grid, each one spaced at 1 mm from the next. We are not in a position to answer the question of cost at the present time. With regard to number of samples, a set of observations would include up to 24 BSE images for a general survey, but with up to a dozen including the X-ray mapping. The acquisition of the latter is the most time consuming, but we normally leave the SEM running unattended during this acquisition.

Reviewer 2: Is it possible to give the compositions of the clay (e.g. kaolinite, smectite) so as to compare with the quartz and feldspar? This would be useful for non-specialists.
Authors: We have yet to determine the bulk clay composition, but this would present no difficulty using X-ray diffraction equipment.